Published in final edited form as:
Cancer Res. 2014 December 15; 74(24): 7285–7297. doi:10.1158/0008-5472.CAN-14-1240.

RAGE Expression in Tumor-associated Macrophages Promotes Angiogenesis in Glioma

Xuebo Chen[#1], **Leying Zhang**[#2], **Ian Y. Zhang**[2], **Junling Liang**[3], **Huaqing Wang**[4], **Mao Ouyang**[5], **Shihua Wu**[3], **Anna Carolina Carvalho da Fonseca**[6], **Lihong Weng**[7], **Yasuhiko Yamamoto**[8], **Hiroshi Yamamoto**[8], **Rama Natarajan**[9], and **Behnam Badie**[2,10]

[1]Department of General Surgery, China Japan Union Hospital of Jilin University, Changchun, Jilin Province, P.R.China

[2] Division of Neurosurgery, City of Hope Beckman Research Institute

[3]Research Center of Siyuan Natural Pharmacy and Biotoxicology, College of Life Sciences, Zhejiang University, Hangzhou, P.R. China

[4]Department of Emergency Surgery, Qilu Hospital of Shandong University, Jinan, Shandong Province, P.R. China

[5]Department of Cardiology, Third Xiangya Hospital, Central South University, Changsha Hunan, P.R. China

[6]Laboratório de Morfogênese Celular, Instituto de Ciências Biomédicas, Universidade Federal do Rio de Janeiro, Rio de Janeiro, Brazil, Bolsista do CNPq

[7]Department of Hematology and Hematopoietic Cell Transplantation, City of Hope Beckman Research Institute

[8]Department of Biochemistry and Molecular Vascular Biology, Kanazawa University, Japan

[9] Division of Molecular Diabetes Research, City of Hope Beckman Research Institute

[10]Department of Cancer Immunotherapeutics & Tumor Immunology, City of Hope Beckman Research Institute

[#] These authors contributed equally to this work.

Abstract

Interaction of RAGE with its ligands can promote tumor progression, invasion and angiogenesis. Although blocking RAGE signaling has been proposed as a potential anti-cancer strategy, functional contributions of RAGE expression in the tumor microenvironment (TME) has not been investigated in detail. Here, we evaluated the effect of genetic depletion of RAGE in TME on the growth of gliomas. In both invasive and non-invasive glioma models, animal survival was prolonged in RAGE knockout ($Ager^{-/-}$) mice. However, the improvement in survival in $Ager^{-/-}$ mice was not due to changes in tumor growth rate but rather to a reduction in tumor-associated

Corresponding Author: Behnam Badie, Division of Neurosurgery, City of Hope, 1500 East Duarte Road Duarte, CA, 91010; Phone: 626-471-7100; Fax: 626-471-7344; bbadie@coh.org.

Conflict of Interests: None

inflammation. Furthermore, RAGE ablation in the TME abrogated angiogenesis by downregulating the expression of pro-angiogenic factors which prevented normal vessel formation, thereby generating a leaky vasculature. These alterations were most prominent in non-invasive gliomas, where the expression of VEGF and pro-inflammatory cytokines were also lower in tumor-associated macrophages (TAM) in $Ager^{-/-}$ mice. Interestingly, reconstitution of $Ager^{-/-}$ TAM with wild-type microglia or macrophages normalized tumor vascularity. Our results establish that RAGE signaling in glioma-associated microglia and TAM drives angiogenesis, underscoring the complex role of RAGE and its ligands in gliomagenesis.

Keywords

Brain tumor; Macrophage; Mice; RAGE

Introduction

With the development of targeted therapies against gliomas, the contribution of tumor microenvironment (TME) to treatment response is becoming clearer. Glioma-associated stromal cells like astrocytes, endothelial cells, mesenchymal cells and infiltrating inflammatory cells play an important role in tumorigenesis, angiogenesis, invasion and immune evasion. Among these cells, infiltrating microglia (MG) and macrophages (MP), (referred to as tumor-associated macrophages or TAMs) have received recent attention due to their involvement in glioma escape from anti-angiogenic agents (1). As components of the innate immune system, TAMs are a heterogeneous cell population that are derived from resident brain MG and myeloid-derived monocytes, and express a variety of pattern recognition receptors that constantly monitor changes in TME. One such receptor is the receptor for advanced glycation end-products (RAGE) that was initially discovered as a membrane protein that binds glycosylated macromolecules.

RAGE has been implicated in a variety of human disease processes (2, 3). Under normal physiological conditions, RAGE is expressed at high levels in the lungs, and at lower levels in a variety of other cell types including immune cells, neurons, activated endothelial and vascular smooth muscle cells. However, in pathophysiological settings such as diabetes, chronic inflammation or neurodegenerative disorders, RAGE expression is increased drastically in other tissues such as vasculature, hematopoietic cells and the central nervous system (CNS) (4).

RAGE binds to a variety of ligands including advanced glycation endproducts (AGEs) and S100 proteins. Furthermore, as a pattern recognition receptor, RAGE binds to proteins such as high mobility group box 1 (HMGB1) that originate from damaged cells and activate the immune system (3). Engagement of RAGE by its ligands results in the activation of multiple downstream signaling pathways which eventually lead to the activation of NF-κB, ERK1/2, p38 and STAT3 and consequent regulation of cytokines, chemokines, adhesion molecules, and pathways that regulate cell proliferation, survival, differentiation, migration, phagocytosis and authophagy (4). Thus, it is not surprising that RAGE signaling has also been implicated in tumorigenesis.

By facilitating the maintenance of a chronic inflammatory state, upregulation of RAGE and its ligands have been linked to the development and progression of several neoplasms including gastric cancer (5), colon cancer (6), pancreatic cancer (7) and prostate cancer (8). Furthermore, blockade of RAGE signaling have been used to inhibit tumor growth, invasion and angiogenesis in a variety of cancers (9-12). One of the earliest reports to demonstrate the therapeutic efficacy of this approach was in gliomas where blockade of RAGE interaction with HMGB1 was shown to inhibit tumor growth and invasion (13). Most studies that have evaluated RAGE signaling in tumors, however, have focused on the RAGE signaling in neoplastic cells, and the contribution of RAGE expression in the TME to tumorigenesis has not been investigated in detail.

The goal of this study was to evaluate the effect of genetic depletion of RAGE in TME on the growth of gliomas. Because gliomas are heterogeneous tumors with both invasive and noninvasive “bulky” phenotypes, two different syngeneic glioma models were used for these experiments. In both glioma models, animal survival was prolonged in *Ager*$^{-/-}$ mice. This improvement in animal survival, however, was not due to changes in tumor growth, but a reduction in tumor-associated inflammation in *Ager*$^{-/-}$ mice. Furthermore, RAGE ablation in TME abrogated angiogenesis by downregulating the expression of pro-angiogenic factors that prevented normal vessel formation. These vascular alterations, however, were most prominent in non-invasive gliomas where the expression of VEGF and pro-inflammatory cytokines was lower in *Ager*$^{-/-}$ TAMs. Interestingly, reconstitution of either RAGE null MG or MP with corresponding WT cells normalized tumor angiogenesis. These findings support the role of TAM RAGE signaling in glioma angiogenesis.

Materials and Methods

Reagents and cell lines

Murine GL261 glioma cells were obtained from Dr. Karen Aboody's laboratory in 2006 and stably transfected with firefly luciferase expression vector as described before (14, 15). Positive clones (GL261-luc) were selected using zeocin (1 mg/mL) and G418. Luciferase-expressing KR158B cells (or K-Luc), an invasive glioma cell line that was derived from spontaneous gliomas in *Trp53/Nf1* double-mutant mice in Dr. Tyler Jacks laboratory, was a generous gift from Dr. John Sampson in 2011 (16). Both GL261 and K-Luc cells were cultured in DMEM medium supplemented with 10% FBS (BioWhittaker, Walkersville, MD), 100 U/mL penicillin-G, 100 μg/mL streptomycin and 0.01 M Hepes buffer (Life Technologies, Gaithersburg, MD) in a humidified 5% CO2 atmosphere, and their tumorigenicity was authenticated by histological characterization of intracranial gliomas in mice.

Tumor implantation and imaging

Mice were housed and handled in accordance to the guidelines and approval of City of Hope Institutional Animal Care and Use Committee under pathogen-free conditions. All mice were on C57BL/6J background. *CX$_3$CR* $^{GFP}{}_1$ Knock-in mice that express EGFP under control of the endogenous Cx3cr1 locus were purchased from Jackson Laboratory (Sacramento, CA). *Ager*$^{-/-}$ mice, a generous gift from Dr. Yasuhiko Yamamoto (Kanazawa

University, Japan), were bred at our institution and PCR genotyped using tail DNA (17). Intracranial (i.c.) tumor implantation was performed stereotactically as described before (18). Briefly, GL261 or K-Luc glioma cells were harvested by trypsinization, counted, and resuspended in culture medium. Female C57BL/6 mice (Jackson Laboratory, Bar Harbor, ME) weighing 15-25 g were anesthetized by intraperitoneal administration of ketamine (132 mg/kg) and xylazine (8.8 mg/kg) and implanted with 10^5 tumor cells using a stereotactic head frame at a depth of 3 mm through a bur hole placed 2 mm lateral and 0.5 mm anterior to the bregma. Tumor growth was assessed by Xenogen IVIS *In Vivo* Imaging System (Xenogen, Palo Alto, CA) as previously described (15).

Real time RT-PCR and Western blot

Real-time quantitative PCR (qPCR) was performed with corresponding primers (Table S1) in a TaqMan 5700 Sequence Detection System (Applied Biosystems, Foster City, CA) as described previously (18).

Western blots were performed as describe before (18) using primary antibodies specific for S100B (Abcam), full length RAGE (FL-RAGE) (Abcam), β-actin (Santa Cruse), S100A9 (R&D Systems), HMGB1 and GAPDH (Cell Signaling).

Cathepsin S assay

Primary bone marrow-derived monocytes (BMM) were harvested from WT and *Ager*$^{-/-}$ mice as described before (19) and cultured in Dulbecco's modified Eagle's medium supplemented with 1% fetal bovine serum, 100 U/ml penicillin-G, 100 μg/mL streptomycin and 0.01 M Hepes. Cathepsin S assay was performed according to the manufacturer's instructions (AnaSpec Inc, Fremont CA, catalog# 72099). Briefly, 10^6 BMM from WT and *Ager*$^{-/-}$ mice were plated in 12-well plated for 24 hours. Cells were then treated with IFNγ (1 μg/ml), or conditioned medium (CM) from GL261or K-Luc cells. Cell lysates were collected at different timepoints and tested for Cathepsin S activity.

RAGE promoter activity assay

A fragment contains the 5'-flanking region (~2000 bp) of the mouse *Ager* (RAGE gene) was generated from mouse genomic DNA by PCR using the following primers: forward, 5'-attgctagcgggaggtcagatatacagtc-3' and reverse, 5'-attaagcttccatctcccatctcgttc-3'. This product was cloned into the NheI and HindIII sites of the pGL3-basic vector (Promega), and the generated plasmid was designated pRAGE-Luc.

Primary BMM from WT and *Ager*$^{-/-}$ mice were cultured in six-well plates as described above. Cells were then transfected with pRAGE-Luc by lipofectamine Reagent (Invitrogen, Carlsbad, CA) for 36 hours and then incubated with CM from GL261 or KLuc cells for 12 hours. Cells were harvested by manual scraping in lysis buffer (Promega) to yield lysates that were then assayed for luciferase activity using Luciferase Assay System (Promega). The luciferase activity was measured in a luminometer.

Vascular permeability

Mice bearing two-week old i.c. GL261 or K-Luc tumors were injected with TRITC-dextran 150 (Life Technology) solution (100 mg/kg i.v.). Brains were harvested after two hours, and fixed in paraformaldehyde for four hours before storage in 30% sucrose solution. Brains were then embedded in O.C.T. (Tissue-Tek), sectioned (10 μm) and baked at 37°C. Images were captured with an AX-70 fluorescent microscopy (Leica Microsystems Inc., Bannockburn, IL) and analyzed by Zeiss LSM Image Browser software.

For Evans blue permeability assay, tumor-bearing mice were anesthetized and injected with Evans blue dye (100 μL of a 1% solution in 0.9% NaCl; Sigma-Aldrich) into the retro-orbital plexus. Thirty minutes later, mice were sacrificed and perfused with PBS. Brains were removed, imaged and dried in 60°C overnight. The Evans blue dye was then extracted using 1 ml formamide at 55°C for 16 hours and quantified with a spectrophotometer at 630 nm (20).

Vascular density

Vascular density was calculated by measuring average vessel diameter over four 10× fields obtained by AX-70 fluorescent microscopy (Leica Microsystems Inc., Bannockburn, IL) and prepared by Zeiss LSM Image Browser software.

Flow cytometry analysis

For *in vivo* staining, tumor tissue was minced and digested with trypsin for 20 minutes at 37°C. Tissue homogenate was then filtered through a 40 μm filter and prepped using Fixation/Permeabilization solution according to the manufacturer's instructions (BD Pharmingen. San Diego, CA). Multiple-color FACS analyses was performed at City of Hope FACS facility using a 3-laser CyAn immunocytometry system (Dako Cytomation, Fort Collins, CO), and data was analyzed using FlowJo software (TreeStar, San Carlos, CA) as described before (19). PerCP-conjugated antibodies to mouse CD45 (Cat: 557235) was purchased from BD Pharmingen (San Diego, CA) Allophycocyaninconjugated anti-mouse CD11b (Cat: 17-0112-82) and the primary rabbit-anti-mouse RAGE (Cat: ab3611-100) were purchased from Abcam (Middlesex, NJ). Secondary goat anti-rabbit-FITC (Cat: sc-2012) and secondary goat anti-mouse-FITC (Cat: sc-2010) were purchased from Santa Cruz Biotechnology (Santa Cruz, CA). Tumor-associated MPs ($CD11b^{high}$ $CD45^{high}$) and MG ($CD11b^{high}$ $CD45^{low}$) were distinguished based on previously described FACS analysis (21).

Bone marrow transplantation

Lethally-irradiated recipient mice (two doses of 550 cGy every four hours) were injected via a tail vein with 5×10^6 bone marrow (BM) cells freshly collected from donor mice. The donor mice were euthanized and BM cells were aseptically harvested by flushing femurs with Dulbecco's PBS (DPBS) containing 2% fetal bovine serum. The samples are combined, filtered through a 40 mm nylon mesh, centrifuged, and passed through a 25 gauge needle. Recovered cells are resuspended in DPBS at a concentration of 5×10^6 viable nucleated cells per 200 μL. All animals were given autoclaved water with sulfatrim from 2 days prior

to 2 weeks after transplantation. Six to eight weeks after transplantation, mice were implanted i.c. with GL261 gliomas.

Immunofluorescence staining

Frozen brain sections were prepared from naive and tumor-bearing mice. Immediately after harvest, brains were fixed in paraformaldehyde for four hours before storage in 30% sucrose solution. Brains were embedded in O.C.T. (Tissue-Tek) and 10 μm sections were cut using cryostat (Leica Microsystem Inc., Bannockburn, IL). Prior to immunofluorescence staining, slides were baked at 37°C and permeabilized in methanol for 15 minuntes. After an one hour block, slides were incubated with Hypoxyprobe-F6 (1:200, Hypoxyprobe, Burlington, MA), RAGE (1:200, rabbit anti-mouse RAGE, Abcam, Middlesex, NJ), CD11b (1:20, rat anti-mouse, Abcam) or CD31 (1:20, rat anti-mouse, Abcam) primary antibodies for 1 hour. Slides were washed with PBS three times for 5 minuntes and incubated with secondary antibody (Goat anti-rabbit Alexa Fluor 555 or Goat anti-mouse Alexa Fluor 555, 1:200 dilution Life Technologies, Carlsbad, CA) for another hour. Tissue sections were mounted in Vectashield mounting medium containing 4060-diamidino-2-phenylindole (DAPI) (Vector, Burlingame, CA), imaged with AX-70 fluorescent microscopy (Leica Microsystems Inc., Bannockburn, IL) and prepared by Zeiss LSM Image Browser software.

For human studies, tumor samples from seven patients with glioblastoma, and peritumoral white matter tissue from one patient were collected under an IRB-approved protocol (IRB 07074), flash-frozen, sectioned (8μm thick), blocked with BSA (0.5% for one hour) before overnight incubation with primary RAGE (1:300, Cat. 3611, Abcam), CD34 (1:100, M7165, Dako) or CD163 (1:100, VP-C374, Vector) antibodies. After washings, slides were incubated with secondary antibodies (donkey anti mouse -A488 and anti rabbit - A555) for one hour and counterstained with DAPI for 5 minutes.

Hypoxia staining

WT or *Ager*$^{-/-}$ mice bearing two-week old i.c. GL261 or K-Luc tumors were injected once with 100mg/kg pimonidazole HCl (100 mg/kg in PBS, i.v.) two hours prior to tissue analysis. Tissue sections were incubated with Hypoxyprobe prior to imaging.

Statistical analysis

Statistical comparison in all different experimental conditions was performed with the GraphPad Prism software using two-way analysis of variance (ANOVA) or Student's t-test. Survival was plotted using a Kaplan-Meir survival curve and statistical significance was determined by the Log-rank (Mantel-Cox) test. A P value of less than 0.05 was considered significant.

Results

RAGE ablation prolongs survival

In order to evaluate the role of RAGE depletion in TME on glioma growth, two different syngeneic orthotopic glioma models were studied. GL261 gliomas grow as “bulky” tumors with only microscopic invasion, while the K-Luc model has a more invasive phenotype. In

both models, animal survival was modesty, but significantly prolonged in *Ager*$^{-/-}$ mice when compared to WT controls (Fig. 1A). This improved survival correlated with slower tumor growth in the GL261, but not the K-Luc model (Fig. 1A lower panel). Interestingly, even with improvement in animal survival, tumor sizes were similar (Fig. 1B), and except for increased necrosis in the *Ager*$^{-/-}$ GL261 gliomas, tumor histology and invasion pattern was unchanged in the *Ager*$^{-/-}$ mice (Fig. 1C). These findings suggested that tumor response to RAGE ablation in TME was different in each glioma model, and other factors besides tumor growth were responsible for improved survival of tumor-bearing *Ager*$^{-/-}$ mice. Because RAGE signaling has been implicated in tumorigenesis, we next evaluated the expression of RAGE and its ligands in each model.

Expression of RAGE and its ligands in gliomas

RAGE engagement by its ligands can lead to induction of NF-κB and activation of inflammatory pathways that further upregulate RAGE expression and its ligands in a feed-forward mechanism (3). As a result, ablation of RAGE in TME may impair RAGE/ligand interactions in tumor leukocytes and abrogate tumor inflammation. Alternatively, RAGE ablation in TME may also decrease the release of soluble RAGE (sRAGE). sRAGE serves as a decoy receptor, and by binding to ligands in the extracellular space, antagonizes the activation of RAGE (22). Thus, by reducing sRAGE in TME, more ligands will be available to activate tumor RAGE in an autocrine fashion. To study this complex interaction *in vivo*, we first confirmed the expression of RAGE and its ligands in each glioma model. As expected, RAGE expression was markedly lower in the lungs and brains of *Ager*$^{-/-}$ mice (Fig. 2A). Very low levels of RAGE staining in the *Ager*$^{-/-}$ brains (neurons) and lungs most likely represented expression of other RAGE isoforms that were not depleted in the *Ager*$^{-/-}$ model and/or due to non-specific binding of the primary RAGE antibody (Fig. 2A, lower panel). Although each cell line expressed similar levels of FL-RAGE *in vitro* (Fig. 2B), RAGE expression in i.c. tumors was different in each mouse strain. In GL261 tumors, FL-RAGE levels were similar in WT and *Ager*$^{-/-}$ mice (Fig. 2C, left panel), but in the K-Luc tumors, it was slightly higher in *Ager*$^{-/-}$ mice (Fig. 2C, right panel). Considering that nuclear RAGE levels were similar in WT and *Ager*$^{-/-}$ tumors (Fig. 2D), higher FL-RAGE protein in *Ager*$^{-/-}$ K-Luc tumors (Fig. 2C) most likely represented higher membrane-bound RAGE or sRAGE levels that were not detectable by immunohistochemistry. Because RAGE signaling can directly modulate the expression of its ligands, we next measured the levels of known glioma RAGE ligands in these models.

To assess RAGE ligands, i.c. tumors were separated from surrounding brain tissue and analyzed by Western. In the normal brains, levels of all the ligands were slightly lower in *Ager*$^{-/-}$ mice, confirming the abrogation of the RAGE feed-forward regulation of its ligand production (Fig. 2E). Interesting, the expression profile of RAGE ligands was different between the two glioma models; although K-Luc tumors expressed lower S100B levels than GL261 gliomas, these tumors had higher levels of pro-inflammatory ligands such as HMGB1 and S100A9. High levels of HMGB1 and pro-inflammatory S100 proteins have been implicated in tumor invasion (23), possibly accounting for the phenotypic differences between these two models. Furthermore, the expression of common RAGE ligands was similar in WT and *Ager*$^{-/-}$ mice in both tumor models. Thus, the impact of RAGE ablation

on animal survival was most likely due to modulation of TME and not alterations of RAGE signaling in tumor cells. Because inflammation has been shown to promote tumor progression in a variety of cancers (24), we next studied leukocyte trafficking in each glioma model.

Impact of RAGE ablation on tumor inflammatory response

In order to evaluate the role of RAGE in leukocyte trafficking into tumors, *Ager*$^{-/-}$ $CX_3CR\ ^{GFP}{}_1$ mice were generated and implanted with each glioma model. Surprisingly, RAGE ablation in TME did not alter leukocyte trafficking or distribution in either GL261 or K-Luc tumors (Fig. 3A), and the proportion of inflammatory cells (i.e. lymphocytes, MG and MP) in each tumor type was similar in the WT and *Ager*$^{-/-}$ mice (Fig. 3B). This suggested that RAGE did not play an important role in leukocyte chemoattraction in these glioma models. However, when tumor cytokines were examined, both tumor models had lower expression of pro-inflammatory cytokines (IL-6, IL-1β and TNFα) in *Ager*$^{-/-}$ mice (Fig. 3C). These findings are consistent with the pro-inflammatory functions of RAGE and indicate that suppression of inflammation may have abrogated tumor growth and accounted for the improved survival of glioma-bearing *Ager*$^{-/-}$ mice. Because RAGE signaling has also been implicated in tumor angiogenesis, we next evaluated the expression of angiogenic factors in each model.

Impact of RAGE on angiogenesis

Besides pro-inflammatory cytokines, tumors in *Ager*$^{-/-}$ mice also expressed lower levels of pro-angiogenic factors (Fig. 4A). Although MMP2, a metalloproteinase that is involved in glioma invasion and angiogenesis (25), was also expressed at lower levels in *Ager*$^{-/-}$ mice, tumor invasive phenotypes were similar in both mouse stains (Fig. 1C). Because histological analysis of tumors had demonstrated RAGE expression in tumor vessels (Supplementary Fig. 1S), we next evaluated the vascular density in each tumor type. While pro-anigogenic factors appeared to be suppressed in both glioma models in *Ager*$^{-/-}$ mice, only the GL261 tumors had an obvious vascular phenotypic change with large dilated vessels (Fig. 4B and Supplementary Fig. 2S). Furthermore, GL261 tumors that typically grow as a “bulky” mass appeared to be more hypoxic in *Ager*$^{-/-}$ mice than in WT animals (Fig. 4C). The more invasive K-Luc gliomas, on the other hand, had no signs of hypoxia and exhibited normal vascular characteristics. This finding was consistent with the histological data demonstrating central necrosis in large GL261 gliomas in *Ager*$^{-/-}$ mice (Fig. 1C). Furthermore, poor perfusion of the GL261 gliomas in *Ager*$^{-/-}$ mice may have prevented the uptake of luciferin by tumors, thus accounting for the discrepancy between the tumor luciferase activity (Fig. 1A) and tumor size (Fig. 1B).

In addition to changes in vascular morphology, GL261 vessels also were more permeable in *Ager*$^{-/-}$ mice (Fig. 4D and E). K-Luc vessels also appeared to be leakier in *Ager*$^{-/-}$ mice, but this higher permeability did not translate into a statistically significant increase in overall tumor permeability (Fig. 4D and E).

In summary, the impact of RAGE ablation in TME on the growth of gliomas appeared to be due to a decrease in tumor inflammation and impairment of angiogenesis. The latter

phenomenon, however, was more apparent in the “bulky” GL261 glioma model that rely on angiogenesis and not the more invasive K-Luc model. To assess the significance of these findings to human tumors, we then evaluated RAGE expression in freshly harvested malignant glioma tumor samples.

RAGE expression in human malignant gliomas

RAGE expression was evaluated in seven histologically-confirmed glioblastoma samples (grade IV astrocytomas) and white matter tissue harvested from “tumor edge”. All gliomas, but not cells in the ”tumor edge”, expressed high levels of RAGE (Fig. 5A and B). RAGE expression was also detected in both tumor vessels ($CD34^+$) and TAMs ($CD163^+$) in every glioma sample (Fig. 5C). Nearly half of TAMs expressed RAGE in each sample. Because TAMs are prominent component of TME and play an important role in tumor angiogenesis (26) we evaluated their angiogenic properties following RAGE ablation.

Role of TAM RAGE expression on angiogenesis

As we reported previously, RAGE was expressed by both CNS MG and myeloid-derived MP in GL261 gliomas (Fig. 6A) (18). Furthermore, the proportion of $RAGE^+$ MG (50-60%) and MP (~20%) in the GL261 model was very similar to the average proportion of $RAGE^+$ TAMs in the human glioblastoma samples (50-60%). To evaluate the impact of RAGE ablation in these cells, TAMs from i.c. GL261 gliomas were isolated and analyzed by qPCR. As expected, TAMs that originated from $Ager^{-/-}$ mice had lower expression of IL-6 and VEGF-α (Fig. 6B). Also, as compared to WT cells, BMM isolated from $Ager^{-/-}$ mice expressed lower levels of MMP9 (Fig. 6C) and Cathepsin S (Fig. 6D) when they were exposed to GL261 CM but not K-Luc CM. Finally, RAGE signaling was significantly attenuated in $Ager^{-/-}$ MPs in response to CM from either GL261 or K-Luc cells (Fig. 6C), confirming activation of RAGE by glioma-derived factors in both models. However, in comparison to $Ager^{-/-}$ BMM that were exposed to GL261 factors, *Ager* promoter activity was not completely abolished in the cells that were incubated with KLuc CM, most likely due to activation of other RAGE-independent pathways by pro-inflammatory RAGE ligands (like HMGB1). Overall, these findings suggest that TAM RAGE activation was more important in angiogenesis in GL261 tumor, but not in the more invasive K-Luc gliomas.

TAMs in gliomas are derived from CNS MG and circulating myeloid-derived cells such as monocytes. In order to evaluate the angiogenic function of RAGE in each cell type, chimeric mice were generated prior to tumor implantation. The feasibility of this technique was first assessed by cross transplanting BM from $CX_3CR^{GFP}{}_1$ and WT mice. After recovery, mice were implanted with GL261 tumors and analyzed by histochemistry and flow cytometry. Glioma MPs were identified as $CD45^{high}$ $CD11b^{high}$ cells as we reported before (21), and appeared to infiltrate into the tumors (Fig. 7A, left panel). In the reverse transplantation experiments, where recipient mice were $CX_3CR^{GFP}{}_1$, tumor MG were identified as $CD45^{intermediate}$ $CD11b^{high}$ cells and mostly remained within the margin of the tumor (Fig. 7A, right panel).

To evaluate the impact of MP RAGE expression on tumor angiogenesis, $Ager^{-/-}$ mice were then used as donor BM. Total tumor VEGF-α expression was significantly lower in these

mice (Fig. 7B), but this VEGF decline was not as profound as when tumors were propagate in *Ager*$^{-/-}$ mice (Fig. 4A), suggesting that other myeloid-derived cells (like MG) from WT recipient mice may have also contributed to tumor VEGF-α production. To confirm this, tumor vascular density was compared in cross transplant experiments (Fig. 7C). Interestingly, only mice that lacked RAGE expression in both MG and MP demonstrated large dilated vessels confirming that RAGE expression by either tumor MG or MP was sufficient to normalize angiogenesis in GL261 tumors.

Discussion

Interaction of RAGE with its ligands through both autocrine and paracrine mechanisms can enhance tumor progression, invasion and angiogenesis, and blockage of this interaction has been proposed as a potential anti-cancer therapy (27). In the current study, we demonstrate that genetic ablation of RAGE in TME also prolonged survival of glioma-bearing mice by reducing tumor-associated inflammation and angiogenesis. The survival benefit of RAGE ablation in TME, however, was modest and its function in angiogenesis was dependent on tumor phenotype. In less invasive GL261 gliomas that grow as “bulky” tumors, RAGE ablation in TAMs reduced vascular remodeling, leading to dilated vessels, tumor hypoxia and necrosis. In the more invasive K-Luc model, on the other hand, RAGE blockade did not have a significant impact on tumor angiogenesis. To our knowledge, this is the first report to demonstrate the pro-angiogenic function of RAGE signaling in tumor macrophages. Our findings also emphasize the complex role of RAGE and its ligands in gliomagenesis.

We expected RAGE ablation in TME to inhibit leukocyte trafficking into gliomas because RAGE may function as an adhesion molecule (28) and aid leukocyte recruitment by binding to CD11b (29, 30). Furthermore, RAGE has been shown to be important in S100B-mediated chemoattraction of MG (31). In the current study, however, RAGE expression did not inhibit TAM infiltration in gliomas. This finding is consistent with our recent report demonstrating that S100B-mediated promotion of leukocyte trafficking into gliomas was not dependent on RAGE expression in TME, but mediated through upregulation of CCL2 (32). Similarly, Heijmans et al reported that lack of RAGE in colon polyps did not influence MP trafficking, but instead, caused a marked increase in infiltrating mast cells (33). These results support the presence of multiple overlapping pathways that promote TAM chemoattraction into tumors.

Although RAGE did not affect MP trafficking, its blockade abrogated tumor inflammation and improved survival of two phenotypically different glioma models. As a multiligand receptor, activation of RAGE can upregulate the expression of pro-inflammatory cytokines (4). Consistent with these reports, we noted a decrease in inflammatory cytokines in both invasive and non-invasive gliomas in *Ager*$^{-/-}$ mice. Suppression of tumor inflammation was most likely due to inactivation of RAGE on TAMs and not modulation of RAGE in tumor cells because levels of RAGE ligands did not significantly change in *Ager*$^{-/-}$ mice. Nevertheless, reduction of tumor inflammation was sufficient to modesty improve survival of glioma-bearing *Ager*$^{-/-}$ mice.

RAGE ablation in TME also affected angiogenesis in both glioma models. Tumors in *Ager*$^{-/-}$ mice had more permeable blood vessels and lower expression of proangiogenic factors. Circulating AGEs can contribute to vascular remodeling processes associated with inflammation and cancer (23, 34). Furthermore, RAGE is expressed by vascular smooth muscle and endothelial cells where its activation by RAGE ligands results in their proliferation, migration and tube formation (35-37). Also, Spiekerkoetter et al. reported that S100A4 (a RAGE ligand) activates the MAPK pathway via RAGE, leading to the expression of MMP2, which is essential for vascular smooth muscle cell migration (38). Thus, in both glioma models, development of permeable vessels may have been due to direct RAGE ablation in vascular smooth muscle and endothelial cells. However, while tumor vessels were more permeable in *Ager*$^{-/-}$ mice, angiogenesis was more perturbed in the GL261 model where vascular remodeling was diminished, resulting in poor tumor perfusion and central necrosis.

In contrast to K-Luc tumors, GL261 gliomas in *Ager*$^{-/-}$ mice were more hypoxic and necrotic due to their “bulky” phenotype and dependency on angiogenesis for growth. In these tumors, RAGE expression was necessary for vascular normalization and remodeling that was essential to tumor perfusion. The exact mechanism by which RAGE signaling in GL261 TAMs regulated angiogenesis remains unclear, but our data suggests that expression of proteinases may play a role in this process. BMM from *Ager*$^{-/-}$ mice expressed lower levels of MMP9 and Cathepsin S when incubated with GL261 CM. These proteases are secreted by MG and MPs (26, 39, 40), are important in CNS tissue remodeling and have been shown to play a role in glioma angiogenesis and invasion (25, 41, 42). Interestingly, in GL261 gliomas, RAGE expression by both resident MG and infiltrating monocytes was important for angiogenesis in these tumors, suggesting that therapeutic strategies that only target infiltrating monocytes (and not MG) may not be adequate in preventing angiogenesis in these tumors.

In addition to RAGE activation in TAMs, variation in the expression of RAGE ligands may have differently impacted tumor angiogenesis in response to RAGE ablation in each model. The K-Luc model expressed high levels of HMGB1 and S100A9, which enhance tumor invasion, migration and angiogenesis (43). High levels of HMGB1 expression by K-Luc gliomas may have overcome the dependency on RAGE signaling for angiogenesis in this model. Besides RAGE, HMGB1 has been shown to bind other receptors such as TLR4 and TLR2 (44, 45). Activation of these receptors by HMGB1 that was secreted by K-Luc cells may have been responsible for stimulation of the RAGE pathway through a RAGE-independent mechanism. Perhaps inhibition of HMGB1 production in this model may be a more potent anti-angiogenic strategy than inhibiting RAGE signaling.

In summary, this study demonstrates the role of TAM RAGE expression in glioma angiogenesis, and highlights the diversity of RAGE signaling in these heterogeneous tumors. Although RAGE ablation in TME by itself my not be a viable treatment for malignant gliomas, targeting the interaction of RAGE ligands with their receptors may have therapeutic potential.

Supplementary Material

Refer to Web version on PubMed Central for supplementary material.

Acknowledgements

The authors thank Brian Armstrong for assisting with fluorescent microscopy.

Grant Support: This work was supported by R01 CA155769, R21 NS081594 and R21 CA189223 (to BB), and R01DK065073 (to RN). The City of Hope Flow Cytometry Core was equipped in part through funding provided by ONR N00014-02-1 0958, DOD 1435-04-03GT-73134, and NSF DBI-9970143.

References

1. Piao Y, Liang J, Holmes L, Zurita AJ, Henry V, Heymach JV, et al. Glioblastoma resistance to anti-VEGF therapy is associated with myeloid cell infiltration, stem cell accumulation, and a mesenchymal phenotype. Neuro Oncol. 2012; 14:1379–92. [PubMed: 22965162]
2. Ramasamy R, Yan SF, Schmidt AM. RAGE: therapeutic target and biomarker of the inflammatory response--the evidence mounts. J Leukoc Biol. 2009; 86:505–12. [PubMed: 19477910]
3. Sorci G, Riuzzi F, Giambanco I, Donato R. RAGE in tissue homeostasis, repair and regeneration. Biochim Biophys Acta. 2013; 1833:101–9. [PubMed: 23103427]
4. Kierdorf K, Fritz G. RAGE regulation and signaling in inflammation and beyond. J Leukoc Biol. 2013
5. Kuniyasu H, Oue N, Wakikawa A, Shigeishi H, Matsutani N, Kuraoka K, et al. Expression of receptors for advanced glycation end-products (RAGE) is closely associated with the invasive and metastatic activity of gastric cancer. J Pathol. 2002; 196:163–70. [PubMed: 11793367]
6. Fuentes MK, Nigavekar SS, Arumugam T, Logsdon CD, Schmidt AM, Park JC, et al. RAGE activation by S100P in colon cancer stimulates growth, migration, and cell signaling pathways. Dis Colon Rectum. 2007; 50:1230–40. [PubMed: 17587138]
7. Takada M, Koizumi T, Toyama H, Suzuki Y, Kuroda Y. Differential expression of RAGE in human pancreatic carcinoma cells. Hepatogastroenterology. 2001; 48:1577–8. [PubMed: 11813576]
8. Ishiguro H, Nakaigawa N, Miyoshi Y, Fujinami K, Kubota Y, Uemura H. Receptor for advanced glycation end products (RAGE) and its ligand, amphoterin are overexpressed and associated with prostate cancer development. Prostate. 2005; 64:92–100. [PubMed: 15666359]
9. Xu XC, Abuduhadeer X, Zhang WB, Li T, Gao H, Wang YH. Knockdown of RAGE inhibits growth and invasion of gastric cancer cells. European journal of histochemistry : EJH. 2013; 57:e36. [PubMed: 24441189]
10. Yaser AM, Huang Y, Zhou RR, Hu GS, Xiao MF, Huang ZB, et al. The Role of Receptor for Advanced Glycation End Products (RAGE) in the Proliferation of Hepatocellular Carcinoma. Int J Mol Sci. 2012; 13:5982–97. [PubMed: 22754344]
11. Elangovan I, Thirugnanam S, Chen A, Zheng G, Bosland MC, Kajdacsy-Balla A, et al. Targeting receptor for advanced glycation end products (RAGE) expression induces apoptosis and inhibits prostate tumor growth. Biochem Biophys Res Commun. 2012; 417:1133–8. [PubMed: 22206663]
12. DiNorcia J, Lee MK, Moroziewicz DN, Winner M, Suman P, Bao F, et al. RAGE gene deletion inhibits the development and progression of ductal neoplasia and prolongs survival in a murine model of pancreatic cancer. J Gastrointest Surg. 2012; 16:104–12. discussion 12. [PubMed: 22052106]
13. Taguchi A, Blood DC, del Toro G, Canet A, Lee DC, Qu W, et al. Blockade of RAGE-amphoterin signalling suppresses tumour growth and metastases. Nature. 2000; 405:354–60. [PubMed: 10830965]
14. Alizadeh D, Zhang L, Hwang J, Schluep T, Badie B. Tumor-associated macrophages are predominant carriers of cyclodextrin-based nanoparticles into gliomas. Nanomedicine. 2010; 6:382–90. [PubMed: 19836468]

15. Alizadeh D, Zhang L, Brown CE, Farrukh O, Jensen MC, Badie B. Induction of anti-glioma natural killer cell response following multiple low-dose intracerebral CpG therapy. Clin Cancer Res. 2010; 16:3399–408. [PubMed: 20570924]
16. Terada K, Wakimoto H, Tyminski E, Chiocca EA, Saeki Y. Development of a rapid method to generate multiple oncolytic HSV vectors and their in vivo evaluation using syngeneic mouse tumor models. Gene Ther. 2006; 13:705–14. [PubMed: 16421599]
17. Myint KM, Yamamoto Y, Doi T, Kato I, Harashima A, Yonekura H, et al. RAGE control of diabetic nephropathy in a mouse model: effects of RAGE gene disruption and administration of low-molecular weight heparin. Diabetes. 2006; 55:2510–22. [PubMed: 16936199]
18. Zhang L, Liu W, Alizadeh D, Zhao D, Farrukh O, Lin J, et al. S100B attenuates microglia activation in gliomas: possible role of STAT3 pathway. Glia. 2011; 59:486–98. [PubMed: 21264954]
19. Zhao D, Alizadeh D, Zhang L, Liu W, Farrukh O, Manuel E, et al. Carbon nanotubes enhance CpG uptake and potentiate antiglioma immunity. Clin Cancer Res. 2011; 17:771–82. [PubMed: 21088258]
20. Zhang H, He Y, Dai S, Xu Z, Luo Y, Wan T, et al. AIP1 functions as an endogenous inhibitor of VEGFR2-mediated signaling and inflammatory angiogenesis in mice. J Clin Invest. 2008; 118:3904–16. [PubMed: 19033661]
21. Badie B, Schartner JM. Flow cytometric characterization of tumor-associated macrophages in experimental gliomas. Neurosurgery. 2000; 46:957–61. discussion 61-2. [PubMed: 10764271]
22. Yonekura H, Yamamoto Y, Sakurai S, Petrova RG, Abedin MJ, Li H, et al. Novel splice variants of the receptor for advanced glycation end-products expressed in human vascular endothelial cells and pericytes, and their putative roles in diabetes-induced vascular injury. Biochem J. 2003; 370:1097–109. [PubMed: 12495433]
23. Sparvero LJ, Asafu-Adjei D, Kang R, Tang D, Amin N, Im J, et al. RAGE (Receptor for Advanced Glycation Endproducts), RAGE ligands, and their role in cancer and inflammation. J Transl Med. 2009; 7:17. [PubMed: 19292913]
24. Grivennikov SI, Greten FR, Karin M. Immunity, inflammation, and cancer. Cell. 2010; 140:883–99. [PubMed: 20303878]
25. Rao JS. Molecular mechanisms of glioma invasiveness: the role of proteases. Nat Rev Cancer. 2003; 3:489–501. [PubMed: 12835669]
26. Du R, Lu KV, Petritsch C, Liu P, Ganss R, Passegue E, et al. HIF1alpha induces the recruitment of bone marrow-derived vascular modulatory cells to regulate tumor angiogenesis and invasion. Cancer Cell. 2008; 13:206–20. [PubMed: 18328425]
27. Musumeci D, Roviello GN, Montesarchio D. An overview on HMGB1 inhibitors as potential therapeutic agents in HMGB1-related pathologies. Pharmacol Ther. 2014; 141:347–57. [PubMed: 24220159]
28. Sessa L, Gatti E, Zeni F, Antonelli A, Catucci A, Koch M, et al. The Receptor for Advanced Glycation End-Products (RAGE) Is Only Present in Mammals, and Belongs to a Family of Cell Adhesion Molecules (CAMs). PLoS One. 2014; 9:e86903. [PubMed: 24475194]
29. Zen K, Chen CX, Chen YT, Wilton R, Liu Y. Receptor for advanced glycation endproducts mediates neutrophil migration across intestinal epithelium. J Immunol. 2007; 178:2483–90. [PubMed: 17277156]
30. Frommhold D, Kamphues A, Hepper I, Pruenster M, Lukic IK, Socher I, et al. RAGE and ICAM-1 cooperate in mediating leukocyte recruitment during acute inflammation in vivo. Blood. 2010; 116:841–9. [PubMed: 20407037]
31. Bianchi R, Kastrisianaki E, Giambanco I, Donato R. S100B protein stimulates microglia migration via RAGE-dependent up-regulation of chemokine expression and release. J Biol Chem. 2011; 286:7214–26. [PubMed: 21209080]
32. Wang H, Zhang L, Zhang IY, Chen X, Da Fonseca A, Wu S, et al. S100B promotes glioma growth through chemoattraction of myeloid-derived macrophages. Clin Cancer Res. 2013; 19:3764–75. [PubMed: 23719262]
33. Heijmans J, Buller NV, Hoff E, Dihal AA, van der Poll T, van Zoelen MA, et al. Rage signalling promotes intestinal tumourigenesis. Oncogene. 2013; 32:1202–6. [PubMed: 22469986]

34. Sakaguchi T, Yan SF, Yan SD, Belov D, Rong LL, Sousa M, et al. Central role of RAGE-dependent neointimal expansion in arterial restenosis. J Clin Invest. 2003; 111:959–72. [PubMed: 12671045]
35. Meloche J, Paulin R, Courboulin A, Lambert C, Barrier M, Bonnet P, et al. RAGE-dependent activation of the oncoprotein Pim1 plays a critical role in systemic vascular remodeling processes. Arterioscler Thromb Vasc Biol. 2011; 31:2114–24. [PubMed: 21680901]
36. Takino J, Yamagishi S, Takeuchi M. Glycer-AGEs-RAGE signaling enhances the angiogenic potential of hepatocellular carcinoma by upregulating VEGF expression. World J Gastroenterol. 2012; 18:1781–8. [PubMed: 22553402]
37. Wang K, Zhou Z, Zhang M, Fan L, Forudi F, Zhou X, et al. Peroxisome proliferator-activated receptor gamma down-regulates receptor for advanced glycation end products and inhibits smooth muscle cell proliferation in a diabetic and nondiabetic rat carotid artery injury model. The Journal of pharmacology and experimental therapeutics. 2006; 317:37–43. [PubMed: 16368901]
38. Spiekerkoetter E, Guignabert C, de Jesus Perez V, Alastalo T-P, Powers J, Wang L, et al. S100A4 and bone morphogenetic protein-2 codependently induce vascular smooth muscle cell migration via phospho-extracellular signal-regulated kinase and chloride intracellular channel 4. Circulation research. 2009; 105:639. [PubMed: 19713532]
39. Hu F, Ku MC, Markovic D, OD AD, Lehnardt S, Synowitz M, et al. Glioma-associated microglial MMP9 expression is upregulated by TLR2 signaling and sensitive to minocycline. Int J Cancer. 2014
40. Small DM, Burden RE, Jaworski J, Hegarty SM, Spence S, Burrows JF, et al. Cathepsin S from both tumor and tumor-associated cells promote cancer growth and neovascularization. Int J Cancer. 2013; 133:2102–12. [PubMed: 23629809]
41. Flannery T, Gibson D, Mirakhur M, McQuaid S, Greenan C, Trimble A, et al. The clinical significance of cathepsin S expression in human astrocytomas. Am J Pathol. 2003; 163:175–82. [PubMed: 12819022]
42. Joyce JA, Baruch A, Chehade K, Meyer-Morse N, Giraudo E, Tsai FY, et al. Cathepsin cysteine proteases are effectors of invasive growth and angiogenesis during multistage tumorigenesis. Cancer Cell. 2004; 5:443–53. [PubMed: 15144952]
43. van Beijnum JR, Nowak-Sliwinska P, van den Boezem E, Hautvast P, Buurman WA, Griffioen AW. Tumor angiogenesis is enforced by autocrine regulation of high-mobility group box 1. Oncogene. 2013; 32:363–74. [PubMed: 22391561]
44. Hori O, Brett J, Slattery T, Cao R, Zhang J, Chen JX, et al. The receptor for advanced glycation end products (RAGE) is a cellular binding site for amphoterin. Mediation of neurite outgrowth and co-expression of rage and amphoterin in the developing nervous system. J Biol Chem. 1995; 270:25752–61. [PubMed: 7592757]
45. Park JS, Svetkauskaite D, He Q, Kim JY, Strassheim D, Ishizaka A, et al. Involvement of toll-like receptors 2 and 4 in cellular activation by high mobility group box 1 protein. J Biol Chem. 2004; 279:7370–7. [PubMed: 14660645]

Precis

Signaling by a pro-inflammatory receptor in glioma-associated microglia and macrophages drives angiogenesis in the tumor microenvironment, reinforcing interest in this receptor as a therapeutic target in glioma.

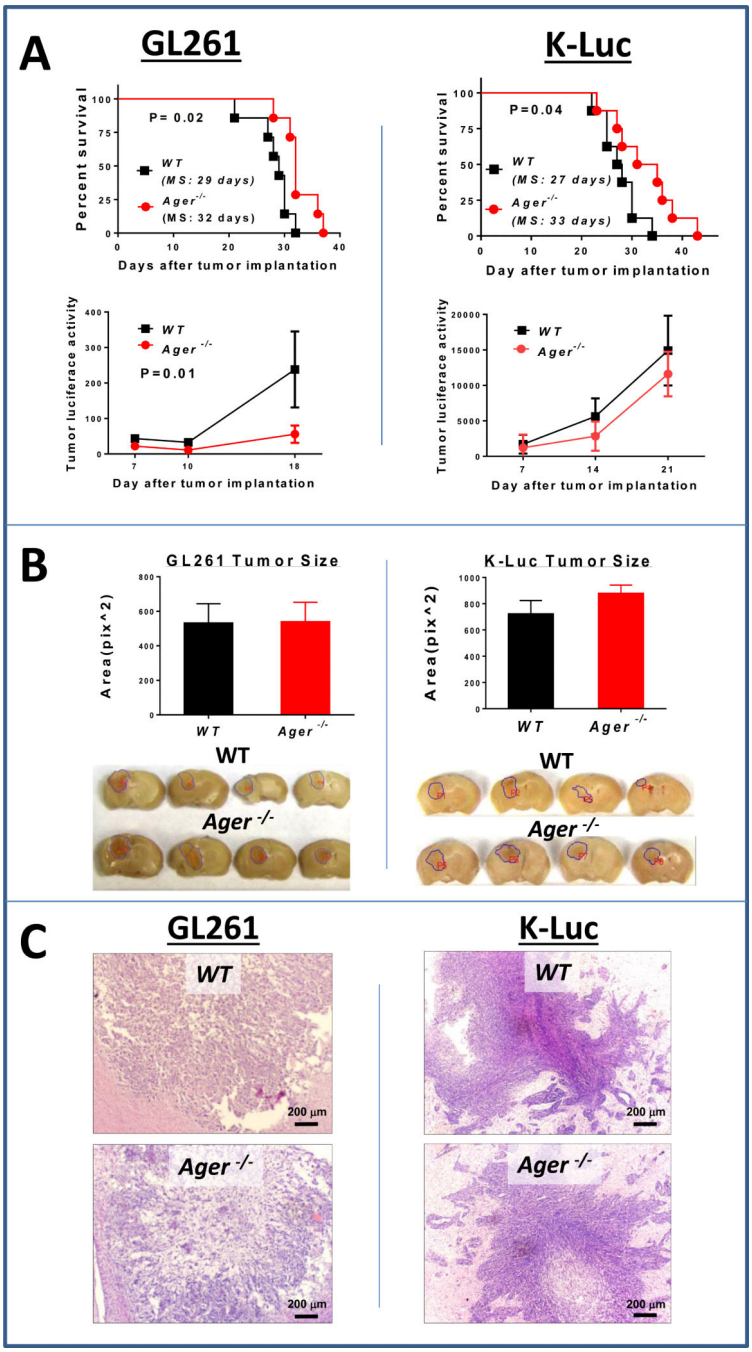

Figure 1.

Impact of RAGE ablation in tumor microenvironment on glioma growth. A, Kaplan-Meier plots (top panel) and tumor luciferase activity (lower panel) in wild-type (WT) and RAGE knockout (*Ager*$^{-/-}$) mice implanted with either intracranial GL261 or KLuc gliomas (n=7-8 mice/group, MS: median survival). B, Despite improvement in survival, tumor size (two weeks after implantation) was similar in WT and *Ager*$^{-/-}$ mice. Cross sections through the largest tumor area were used for size calculations (n=4 mice/group ± SD). C, Except for increased central necrosis in the GL261 tumors in *Ager*$^{-/-}$ mice, tumor histology and

invasion pattern was similar in both strains. Experimental results are representative of three separate experiments.

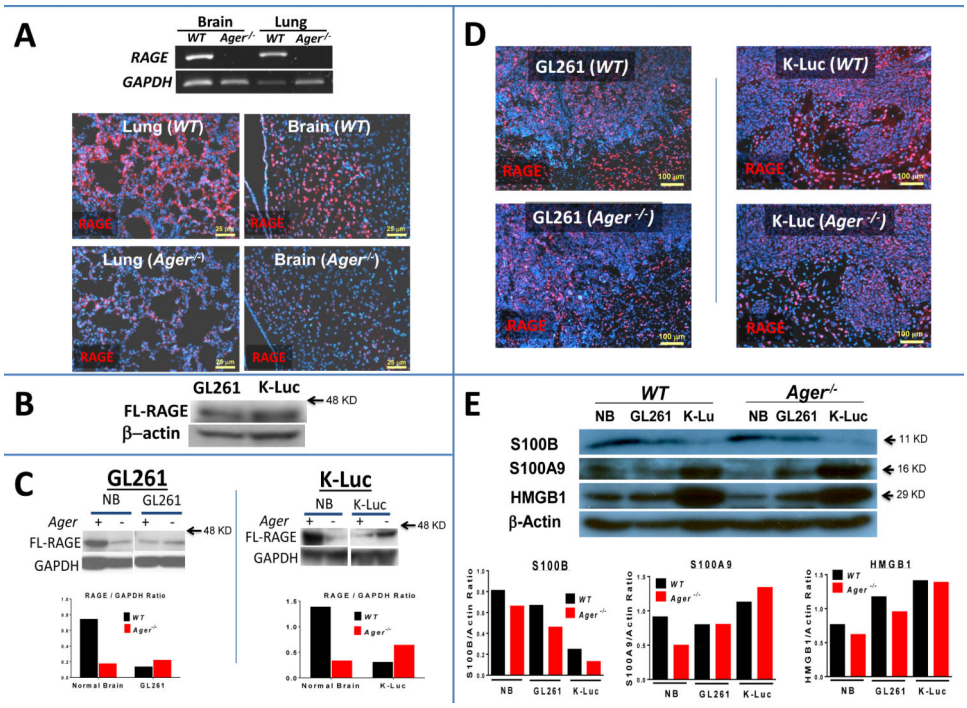

Figure 2.

Expression of RAGE and its ligands in gliomas. A, PCR (top panel) and immunostaining (lower panel) confirming lower RAGE expression in the lungs and brains of non-tumor bearing *Ager*$^{-/-}$ mice. B, Western analysis demonstrating *in vitro* expression of full-length (FL)-RAGE by each cell line prior to implantation. C, FL-RAGE Western blot and D, immunostaining of intracranial GL261 and K-Luc gliomas two weeks after implantation into either WT or *Ager*$^{-/-}$ mice (n=3 mice/group ± SD). E, Western analysis comparing the expression of RAGE ligands by each tumor type two weeks after intracranial implantation. Experimental results are representative of two separate experiments.

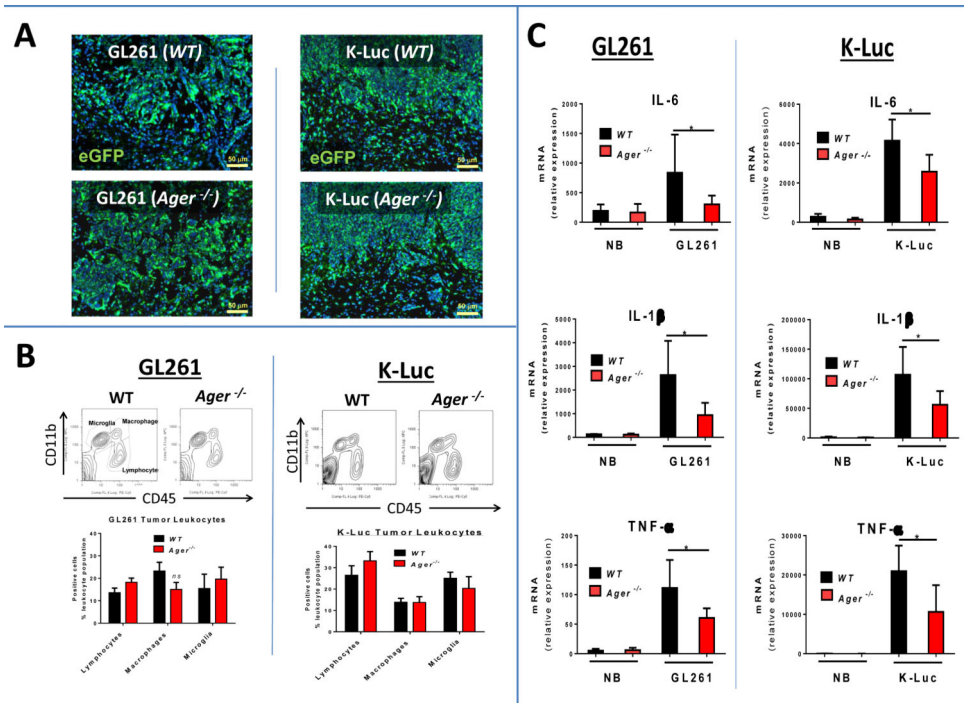

Figure 3.

Impact of RAGE ablation on tumor inflammatory response. A, Infiltration of $CD11b^{+}$ cells (microglia and macrophages) into GL261 and K-Luc gliomas two weeks after intracranial implantation into WT or $Ager^{-/-}$ $CX_3CR_1^{GFP}$ mice. B, Representative flow cytometry contour plots (top) and quantification (bottom) of tumor-associated leukocytes in two-week old intracranial GL261 and K-Luc tumors in WT or $Ager^{-/-}$ mice. (Lymphocytes: $CD45^{+}$, $CD11b^{-}$, microglia: $CD45^{intermediate}$, $CD11b^{high}$, macrophages: $CD45^{+}$, $CD11b^{high}$. n=3 mice/group ± SD). C, qPCR of pro-inflammatory cytokines in normal brain (NB), and intracranial GL261 and K-Luc tumors two weeks after implantation. (n=4 mice/group ± SD), *: $p<0.05$. Experimental results are representative of three separate experiments.

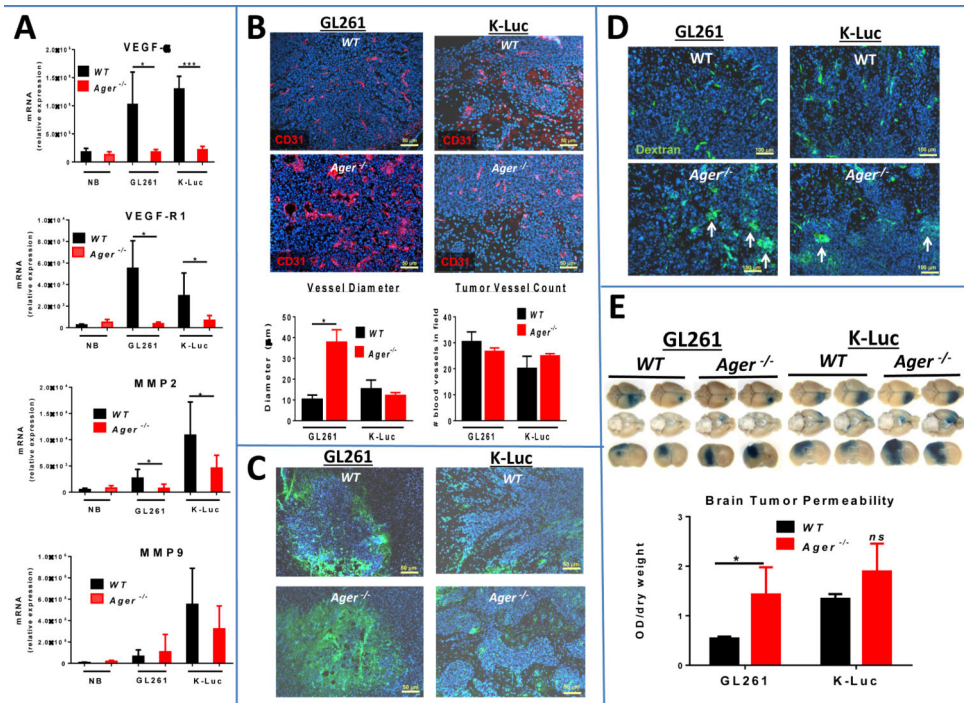

Figure 4.

RAGE ablation abrogates tumor angiogenesis. A, qPCR of normal brain (NB) and intracranial GL261 and K-Luc gliomas demonstrating lower expression of tumor proangiogenic factors in *Ager*$^{-/-}$ mice (n=3 mice/group ± SD). B, Morphology (top panel) and quantification (lower panel) of GL261 and K-Luc blood vessels in WT and *Ager*$^{-/-}$ mice (n=4 mice/group ± SD). C, Tumor hypoxia (green staining) was measured by injecting glioma-bearing mice with pimonidazole two hours prior to tissue examination. Intracranial tumors were harvested two weeks after implantation. D, Effect of RAGE ablation on vascular permeability. Mice bearing two-week old intracranial GL261 or KLuc were injected with TRITC-dextran 150 two hours prior to image analysis. Vascular leakage is evident as dextran extravasation into perivascular space (arrows). E, Tumor vascular permeability was also assessed with Evans blue assay. Tumor-bearing mice were injected with Evans blue dye 30 minutes prior to sample collection. The dye was extracted and quantified with a spectrophotometer. (n=4 mice/group ± SD). *: p<0.05, ***: p<0.001. Experimental results are representative of two separate experiments.

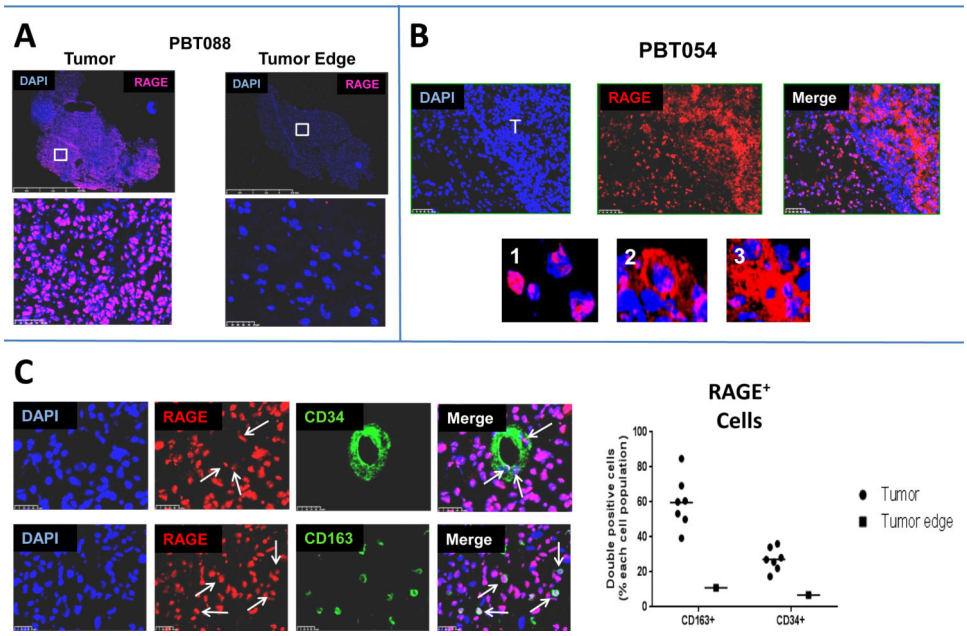

Figure 5.

RAGE expression in human glioblastomas. A, Representative immunohistochemistry of a glioblastoma tumor sample (left panel) and tumor edge (right panel) from the same patient demonstrating RAGE expression in tumor and not peritumoral white matter. B, RAGE expression in another glioblastoma tissue sample demonstrating nuclear (1), membranous (2) and cytoplasmic (3) RAGE expression in tumor cells (T). C, Expression of RAGE in tumor-associated vessels ($CD34^+$, arrows) and macrophages ($CD163^+$, arrows) in a representative glioblastoma sample. Nearly half of the tumor-associated macrophages expressed RAGE in every tumor.

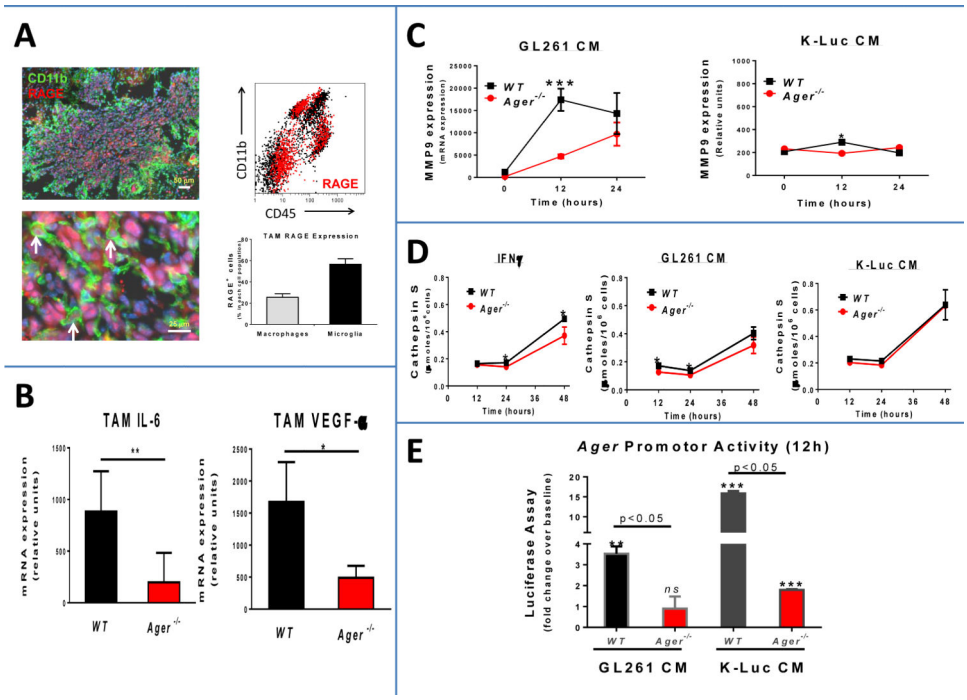

Figure 6.

Effect of RAGE ablation in tumor-associated macrophages (TAMs). A, Representative immunohistochemistry (left panel) and flow cytometry (right panel) of intracranial GL261 tumor in WT mice confirming RAGE expression in TAMs (left: $CD11b^{+}$, arrows; right: red events). Nearly 20% of tumor macrophages $CD45^{high}$ $CD11b^{high}$) and 50% of tumor microglia ($CD45^{intermediate}$ $CD11b^{high}$) expressed RAGE. B, TAM expression of IL6 and VEGFα was suppressed in *Ager*$^{-/-}$ GL261 gliomas. TAMs were isolated by Percoll gradient from intracranial GL261 gliomas two weeks after implantation (n=4 mice/group ± SD). *: p<0.05, **: p<0.01. C, Expression of MMP9 was lower in *Ager*$^{-/-}$ primary bone marrow monocytes (BMM) after incubation with conditioned medium (CM) from GL261 cells. *: p<0.05, ***: p<0.001 D, Cathepsin S expression was modestly lower when *Ager*$^{-/-}$ BMM were incubated with IFNγ and GL261 CM, but not K-Luc CM. *: p<0.05. E, RAGE promotor activity was measured in WT and *Ager*$^{-/-}$ BMM after incubation with CM from GL261 and K-Luc cells. Although *Ager* promotor activity was lower in *Ager*$^{-/-}$ BMM under both conditions, its activity was not completely abolished when cells were exposed to K-Luc CM (n= 4 + SD). **: p<0.01, ***: p<0.001, ns: not significant as compared to cells transfected with control vector. Representative data from two separate experiments is shown.

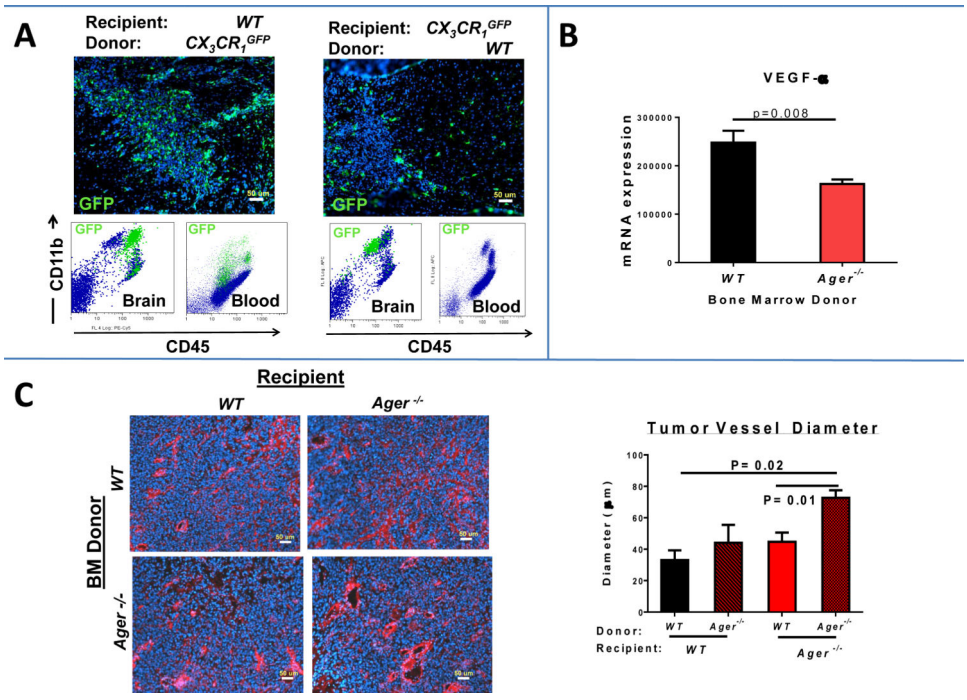

Figure 7.

RAGE ablation in TAMs abrogates angiogenesis in GL261 gliomas. A, To demonstrate the feasibility of generating chimeric mice, bone marrow (BM) cross transplant experiments between wild-type (WT) and $CX_3CR^{GFP}_1$ mice were performed. After recovery, mice were implanted with GL261 tumors and analyzed by histochemistry and flow cytometry. Glioma macrophages were identified as $CD45^{high}$ $CD11b^{high}$ cells (green cells and green events in dot plot) and appeared to infiltrate throughout the tumors (left panel). In the reverse transplantation experiments (right panel) where recipient mice were $CX_3CR^{GFP}_1$, tumor microglia were identified as $CD45^{intermediate}$ $CD11b^{high}$ cells (green events and cells) that mostly remained within the margin of the tumor. B, qPCR demonstrating suppression of VEGFα expression in GL261 tumors that were implanted into WT mice transplanted with $Ager^{-/-}$ BM. C, Tumor vessel characteristics in GL261 gliomas implanted into chimeric mice demonstrating normalization of dialated vessels in mice with either WT microglia or WT macrophages. Representative data from two separate experiments is shown. (n= 3 ± SD). *: $p<0.05$.